Dalton Transactions

RSC Publishing

PAPER

View Article Online
View Journal | View Issue

Cite this: *Dalton Trans.*, 2013, **42**, 12898

Synthesis and structures of Co bis-trifluoromethylpyrazolate complexes†

Joseph H. Rivers and Richard A. Jones*

Received 20th March 2013,
Accepted 15th April 2013

DOI: 10.1039/c3dt50758k

www.rsc.org/dalton

Reactions of $Co(PMe_3)_3Cl$ or $CoCl_2$ with 3,5-$(CF_3)_2$-PzNa in hexane give $Co(PMe_3)_3$(3,5-$(CF_3)_2$-Pz) (**1**) and $Co(PMe_3)_3$(3,5-$(CF_3)_2$-Pz)$_2$ (**2**) respectively (3,5-$(CF_3)_2$-PzNa = sodium bis-trifluoromethylpyrazolate). Reaction of (3,5-$(CF_3)_2$-PzH) with $Co(PMe_3)_4$ produces the unusual complex [*cis*-$Co(PMe_3)_4H_2$][$Co(PMe_3)$(3,5-$(CF_3)_2$-Pz)$_3$] (**3**) which formally contains a $[Co(III)]^+[Co(II)]^-$ complex ion pair. Reaction of 3,5-$(CF_3)_2$-PzLi with an *oxygenated* suspension of $CoCl_2$ and 3 equivalents of PMe_3 gives (3,5-$(CF_3)_2$-Pz)$_2$Co(μ-3,5-$(CF_3)_2$-Pz)(μ-$OPMe_3$)Li($OPMe_3$)$_2$ (**4**), while **2** reacts with LiOH to give [(PMe_3)Co(μ-3,5-$(CF_3)_2$-Pz)$_2$(μ^3-OH)Li]$_2$ (**5**). Both **2** and **3** react with O_2 in toluene solution to give $Co(OPMe_3)_2$(3,5-$(CF_3)_2$-Pz)$_2$ (**6**). All compounds have been characterized spectroscopically and by single crystal X-ray diffraction studies.

Introduction

The microelectronics industry has seen a large push for the development of new materials, some of which involve cobalt based materials to replace current technologies, mainly in copper interconnects. While films of pure metallic cobalt do not make good diffusion barrier layers due to the presence of grain boundaries that allow diffusion of copper, it has been shown that cobalt alloys are promising for use as barrier layers in copper interconnects, especially alloys containing phosphorus.[1] For example, Ekerdt and coworkers recently described the CVD growth of amorphous Co(P) alloys containing 1–5% P from [$Co_2(CO)_8$] and PMe_3 or from the single source precursor [$Co(PMe_3)_4$]. These films been shown to be potential diffusion barrier layers, since they allow virtually no copper diffusion after annealing.[2–4]

Known precursors for the CVD of relatively pure Co films include carbonyl or cyclopentadienyl (Cp) containing complexes. Some of the best studied examples are, $Co_2(CO)_8$, $CoH(CO)_4$, $CoCp_2$, $CoCp(CO)_2$, and $Co(CF_3)(CO)_4$, which have all been used to deposit high purity cobalt films.[5,6] The Cp complexes require the use of H_2 in order to keep the carbon content to a minimum. Several coordination complexes, such as beta-diketonate derivatives (*e.g.* $Co(acac)_2$) and fluorinated analogs such as $Co(hfa)_2$ (hfa = 2,4-$(CF_3)_2$-acetylacetonate) have also been shown to deposit films of cobalt or cobalt oxide.[7,8] The use of alkyl phosphite ligands was shown to produce thermally stable and volatile cobalt complexes of formula, $CoH(P(OR)_3)_4$, (R = Me, Et, *n*-Pr, i-Pr, *n*-Bu, and i-Bu).[9] Thin films grown using these complexes were found to be crystalline films of high purity Co without the need for a reactive gas such as H_2. Single source precursors incorporating more than one metal have also been investigated for the deposition of heterometallic alloys and this is a growing area of research. For example, the complex, $CoGa_2(OtBu)_8$, used as a single source CVD precursor, deposited films of $CoGa_2O_4$.[10] The proposed structure of this complex has the Co and Ga centres bridged by four of the *tert*-butoxide ligands, which may help to distribute the metals evenly throughout the film. A single source CVD precursor, $Ba_2Co(acac)_4(dmae)_3$(dmaeH), for the deposition of Ba_2CoO_3 has also been described which utilizes dimethylaminoethanol (dmae) ligands to bridge Ba and Co. Again, the bonding of both metals within the same molecule may help to create an alloy with evenly distributed metal centres.[11]

We have been interested in exploring the use of alternative ligand systems for the development of new metal complexes as single source precursors for the deposition of metallic films and alloys.[12–15] We and others have shown that the bis-trifluoromethylpyrazolate ligand (3,5-$(CF_3)_2$-Pz) can be used to impart volatility and stability to suitable precursors. For cobalt however, to the best of our knowledge, there appear to be no known examples of cobalt complexes with the 3,5-$(CF_3)_2$-Pz ligand. Moreover, although there are currently over 270 structurally characterized examples of cobalt complexes containing datively or covalently bound pyrazole ligands in the Cambridge database, none appear to be of a cobalt-pyrazolate complex in which the ligand is non-bridging.

We report here the synthesis and structures of new mononuclear 3,5-$(CF_3)_2$-Pz complexes of Co which are stabilized by

Department of Chemistry and Biochemistry, The University of Texas at Austin, Welch Hall 2.204, 105 E. 24th St. STOP A5300, Austin, Texas 78712-1224, USA.
E-mail: rajones@cm.utexas.edu; Tel: +1 (512) 471-1706

†Electronic supplementary information (ESI) available: EPR spectra of **4** and **6** (2 pages). CCDC 887455–887460. For ESI and crystallographic data in CIF or other electronic format see DOI: 10.1039/c3dt50758k

PMe_3. We also describe preliminary testing designed to investigate the potential for these complexes to serve as CVD precursors.

Results and discussion

Synthesis and structures of 1–6

Three new cobalt pyrazolate complexes were synthesized using either standard salt elimination routes from cobalt halides and the sodium or lithium salt of 3,5-$(CF_3)_2$-Pz or by oxidative addition of the N–H bond of the parent pyrazole (3,5-$(CF_3)_2$-PzH) to the highly reactive zero-valent Co complex $Co(PMe_3)_4$ (Scheme 1). The use of *n*-BuLi to generate the pyrazolate lithium salt was the first route explored. However, yields were usually low and the reaction mixtures were extremely air sensitive and prone to atmospheric contamination. The use of NaH to generate the sodium pyrazolate salt resulted in higher yields and was less susceptible to unexpected side reactions. Compounds $Co(PMe_3)_3$(3,5-$(CF_3)_2$-Pz) (**1**) and $Co(PMe_3)_3$(3,5-$(CF_3)_2$-Pz)$_2$ (**2**) were prepared in this manner from $Co(PMe_3)_3Cl$ and $CoCl_2$ respectively. Perhaps the most interesting result came from the addition of the pyrazole (3,5-$(CF_3)_2$-PzH) to $Co(PMe_3)_4$ which resulted in the formation of the unusual complex [*cis*-$Co(PMe_3)_4H_2$][$Co(PMe_3)$(3,5-$(CF_3)_2$-Pz)$_3$] (**3**) which contains a $[Co(III)]^+[Co(II)]^-$ ion pair. The three complexes are extremely sensitive to air and moisture and several new compounds were isolated serendipitously from reactions with the atmosphere. The products were subsequently prepared reproducibly and fully characterized in order to gain further insight into the chemistry of this Co pyrazolate system (Scheme 2).

[$Co(PMe_3)_3$(3,5-$(CF_3)_2$-Pz)] (1). The treatment of a hexane suspension of 3,5-$(CF_3)_2$-PzNa with one equivalent of $Co(PMe_3)_3Cl$ at room temperature and a reaction time of 12 hours resulted in a suspension of NaCl and a blue solution.

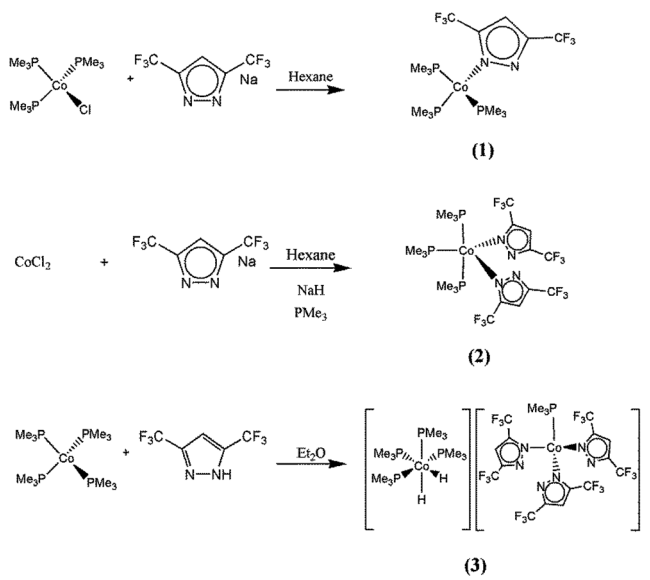

Scheme 1 Synthesis of Co pyrazolate complexes.

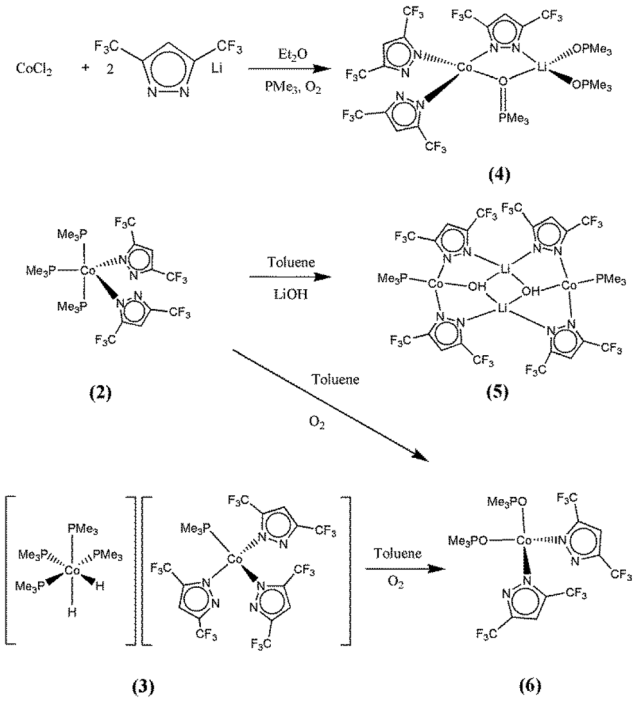

Scheme 2 Reactions of Co pyrazolates with oxygenated species.

After filtration and removal of volatiles *in vacuo*, a dark blue residue remained. This was subjected to sublimation onto a cold finger (−78 °C) under static vacuum (0.1 torr) at 110 °C. The product sublimes readily as a blue crystalline material. The residue was recovered in the glovebox in reasonable yield (68%). On heating under nitrogen (1 atm), **1** melts to a volatile liquid above 80 °C. X-ray diffraction quality single crystals were obtained by slow sublimation in a zone sublimator under static vacuum (0.1 torr) at 110 °C. It is necessary to dry the complex thoroughly before sublimation, as even small amounts of residual solvent inhibit this process with the formation of an oil. Decomposition occurs above 200 °C. Attempts to recrystallize the product from a variety of solvents were unsuccessful because oils form upon cooling.

The compound crystallizes in the chiral monoclinic space group $P2_1$ with two independent molecules in the asymmetric unit, four in the unit cell. The structure is shown in Fig. 1 with crystallographic details given in Table 1 and selected bond lengths and angles in Table 2. The structure features a slightly distorted tetrahedral Co centre. The P–Co–P bond angles are smaller than the idealized 109.5° with an average value of 102.94(3)° while the P(1)–Co(1)–N(1) bond angle is larger than ideal at 133.28(12)°. This distortion is also present in the starting material $Co(PMe_3)_3Cl$, in which the PMe_3 groups point away from the chloride with an average P–Ni–Cl bond angle of 114.07(6)° and an average P–Co–P angle of 104.51(6)°. The Co–P distances (average 2.2358(6) Å) are slightly shorter in **1** than in the starting material which has a unique Co–P bond length of 2.240(6) Å.

The effective magnetic moment of **1** was measured with an Evans method magnetic susceptibility balance at room

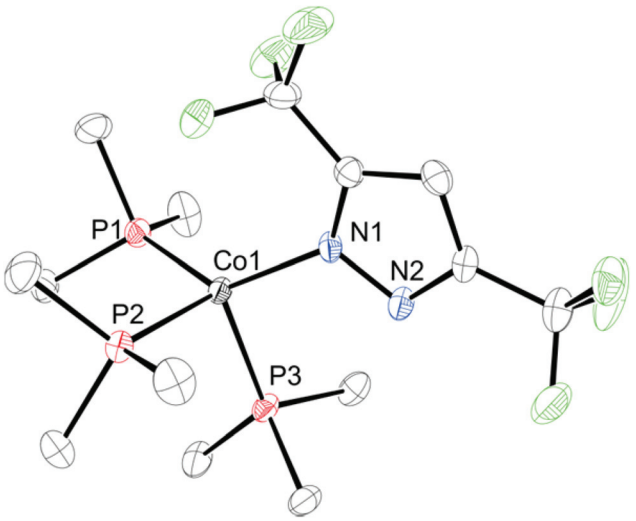

Fig. 1 Molecular structure and atom numbering scheme for $[Co(PMe_3)_3(3,5\text{-}(CF_3)_2\text{-}Pz)]$ (**1**). Thermal ellipsoids are scaled to the 30% probability level. Hydrogen atoms have been omitted for clarity.

temperature in the solid state and found to be $3.055\mu_B$. This is consistent with two unpaired electrons expected for a pseudo-tetrahedral d^8 complex and similar to the value obtained by Klein and Karsch ($3.31\mu_B$) for $Co(PMe_3)_3Cl$ measured in solution. The EPR spectrum for **1** in a frozen toluene solution at 100 K is shown in Fig. 2. Under these conditions, a complex spectrum is observed which is probably due to cobalt fine interactions (I_{Co} = 7/2) and hyperfine couplings between inequivalent phosphorus nuclei (I_P = 1/2) and the N nuclei (I_N = 1). The hyperfine coupling and the deviation of g (g = 2.2472) from that of the free-electron reflect some spin-orbit coupling with the phosphorus nuclei.

$[Co(PMe_3)_3(3,5\text{-}(CF_3)_2\text{-}Pz)_2]$ (2). Treatment of a hexane suspension of two equivalents of 3,5-$(CF_3)_2$-PzNa with a suspension of $CoCl_2$ and 3 equivalents of PMe_3 at room temperature and a reaction time of 12 hours resulted in a suspension of NaCl and a dark blue solution. After filtration and removal of volatiles *in vacuo*, recrystallization of the residue from hexane at −30 °C afforded large brown prisms of **2** in 58% yield which were suitable for X-ray diffraction analysis. The solid is extremely air sensitive and quickly decomposes into a blue oil upon exposure to the atmosphere.

Complex **2** crystallizes in the orthorhombic space group $P2_12_12_1$ with four independent molecules in the unit cell. The structure is shown in Fig. 3 with crystallographic details given in Table 1 and selected angles and bond lengths in Table 3. The inner coordination geometry of the Co center is essentially square pyramidal (or distorted trigonal bipyramidal) which is most likely due to steric interactions between 3,5-$(CF_3)_2$-Pz ligands. The base of the pyramid is formed by the Pz-$(CF_3)_2$ nitrogens, P(2), and P(3), with P(1) in the apical position. The pyrazolate rings are oriented perpendicular to the plane of the base and this minimizes steric interactions between CF_3 and PMe_3 groups. The Co–N bond lengths are similar (1.991(2) Å and 1.990(2) Å) while the Co–P bonds have significantly different values. The Co–P bond lengths in the base are similar for Co(1)–P(2) and Co(1)–P(3) (2.2548(8) Å and 2.2703 (8) Å respectively), while the apical Co(1)–P(1) bond is considerably longer (2.4772(8) Å). The N(1)–Co(1)–N(3) bond angle (164.60(9)°) and the P(2)–Co(1)–P(3) bond angle (173.31(9)°) both approach linearity.

The effective magnetic moment of **2** in the solid state is $1.99\mu_B$ (magnetic susceptibility balance at room temp.). This is consistent with one unpaired electron and expected for a low spin d^7 complex with either square pyramidal or trigonal bipyramidal geometry. The EPR spectrum for **2** collected at 100 K in frozen toluene is shown in Fig. 4. The signal has axial symmetry with g_{avg} = 2.068. Fine coupling to the cobalt nucleus (I_{Co} = 7/2) is apparent, and in the higher magnetic field region, well-resolved hyperfine splitting due to two equivalent phosphorus nuclei (I_P = 1/2, relative intensity 1 : 2 : 1) is observed.

The complex is a low melting solid (m.p. 69–72 °C) under 1 atm N_2, but does not sublime without decomposition. On heating under vacuum (0.1 torr) to assess the volatility, the complex melts in the same range as under N_2, but no change is observed until the temperature reaches 200 °C when a black solid appears above the hot zone.

$[cis\text{-}Co(PMe_3)_4H_2][Co(PMe_3)(3,5\text{-}(CF_3)_2\text{-}Pz)_3]$ (3). The treatment of a diethyl ether solution of $Co(PMe_3)_4$ with approximately 2.6 equivalents of 3,5-$(CF_3)_2$-PzH in diethyl ether at room temperature with a reaction time of 4 hours resulted in a color change of the solution from brown to green and eventually to blue. Removal of the volatiles *in vacuo*, recrystallization of the residue from a mixture of toluene–hexane (9 : 1) and cooling (−30 °C) afforded large purple prisms of **3** in 74% yield which were suitable for X-ray diffraction analysis.

Complex **3** crystallizes in the monoclinic space group $P2_1/n$ with two ion pairs in the asymmetric unit and eight independent ion pairs in the unit cell. The structure of both ions is shown in Fig. 5 with crystallographic details given in Table 1 and selected bond lengths and angles in Table 4. The cationic unit, $[Co(PMe_3)_4H_2]^+$, has been characterized previously in a complex with the $[BPh_4]^-$ anion, though not as a pure complex since it was also substitutionally co-crystallized with $[Co(CO)(PMe_3)_4]^+$ with the dihydride present in 70% of the sites.[16] The distorted octahedral geometry contains the two hydride ligands in a *cis* arrangement consistent with the previous report. The measured angles and distances are consistent with those observed in the previously characterized complex. It is known that metal hydride complexes are often distorted towards the hydride coordination region when the other ligands are bulky. This is observed in **3** with the P(1)–Co(1)–P(4) angle (143.59(7)°) distorted from ideal octahedral geometry. The distortion is also observed for P(2)–Co(1)–P(3) with an angle of 97.33(1)°. The pattern of distortions is consistent with that observed in $[Rh(PMe_3)_4H_2]^+$.[17] The four-coordinate anion, $[Co(PMe_3)(3,5\text{-}(CF_3)_2\text{-}Pz)_3]^-$ adopts a tetrahedral geometry with a slight distortion due to steric crowding of the pyrazolate ligands. This is evident from the N–Co–N angles (112.45(19)–

Table 1 Crystallographic data for compounds **1–6**

	1	**2**	**3**	**4**	**5**	**6**
Empirical formula	$C_{14}H_{28}F_6N_2P_3Co$	$C_{19}H_{29}F_{12}N_4P_3Co$	$C_{30}H_{50}F_{18}N_6P_5Co_2$	$C_{24}H_{30}F_1N_6O_3LiP_3Co$	$C_{26}H_{24}F_{24}N_8O_2Li_2P_2Co_2$	$C_{16}H_{20}F_{12}N_4P_2O_2Co$
Formula weight	490.22	693.3	1109.47	951.32	1130.21	649.23
Temperature (K)	119(2)	100(2)	100(2)	100(2)	100(2)	100(2)
Space group	$P2_1$	$P2_12_12_1$	$P21/n$	$P21/c$	$P\bar{1}$	$P\bar{1}$
Unit cell dimensions						
a (Å)	9.2208(18)	9.3916(8)	10.0753(2)	14.371(3)	9.313(2)	10.1321(13)
b (Å)	16.675(3)	15.6362(12)	68.7275(12)	12.277(3)	11.028(5)	10.2434(13)
c (Å)	15.634(3)	19.3585(16)	13.7230(9)	24.941(8)	11.569(5)	13.9848(17)
α (°)	90	90	90	90	102.591(5)	99.582(3)
β (°)	105.27(3)	90	90.308(6)	115.58(2)	90.458(7)	104.265(4)
γ (°)	90	90	90	90	112.259(17)	101.473(4)
V (Å^3)	2319.0(8)	2842.8(4)	9502.4(7)	3969.1(18)	1067.8(7)	1342.6(3)
Z	4	4	8	4	1	2
D_{calc} (g cm^{-3})	1.404	1.62	1.551	1.592	1.758	1.606
μ (mm^{-1})	0.995	0.869	7.992	0.673	0.994	0.862
$F(000)$	1008	1404	4504	1908	558	650
θ rang (°)	1.82–27.48	3.02–27.48	6.58–69.99	1.81–27.5	3.05–25.0	3.09–25.0
Reflections collected	9975	20 766	152 403	43 036	7085	4713
Unique reflections	9975	6506	17 894	9118	3686	4713
R_{int}	0	0.0476	0.1127	0.0526	0.0518	0
Reflns used	9975	6506	17 894	9118	3686	4713
Restraints	145	0	204	330	120	180
Params	516	361	1201	572	330	399
Goodness-of-fit	1.095	1.058	1.294	1.202	1.099	1.271
Final R indices [$I > 2\sigma(I)$][a]	R_1 = 0.0563	R_1 = 0.0388	R_1 = 0.1018	R_1 = 0.0678	R_1 = 0.0626	R_1 = 0.0852
	wR_2 = 0.1040	wR_2 = 0.0781	wR_2 = 0.1290	wR_2 = 0.1516	wR_2 = 0.1632	wR_2 = 0.2012
R indices (all data)[a]	R_1 = 0.0921	R_1 = 0.0469	R_1 = 0.1697	R_1 = 0.0783	R_1 = 0.0749	R_1 = 0.1158
	wR_2 = 0.1155	wR_2 = 0.0810	wR_2 = 0.1443	wR_2 = 0.1584	wR_2 = 0.1718	wR_2 = 0.2183
Absolute structure parameter	−0.020(15)	0.010(12)				
Largest difference between peak and hole (e A^{-3})	0.907 and −0.376	0.431 and −0.326	0.430 and −0.409	0.470 and −0.657	0.675 and −1.116	0.581 and −0.865

[a] $R_1 = \Sigma_{hkl}(|F_o| - |F_c|)/\Sigma_{hkl}|F_o|$, $R_2 = [\Sigma w(|F_o| - |F_c|)^2/\Sigma w|F_o|^2]^{1/2}$.

Table 2 Selected bond lengths (Å) and angles (°) for **1**

Bond lengths		Bond angles	
Co(1)–N(1)	2.024(4)	N(1)–Co(1)–P(1)	133.28(12)
Co(1)–P(1)	2.2242(14)	N(1)–Co(1)–P(2)	109.13(12)
Co(1)–P(2)	2.2454(15)	P(1)–Co(1)–P(2)	102.41(5)
Co(1)–P(3)	2.2480(13)	N(1)–Co(1)–P(3)	103.04(11)
Co(2)–N(3)	2.021(4)	P(1)–Co(1)–P(3)	103.15(5)
Co(2)–P(4)	2.2373(17)	P(2)–Co(1)–P(3)	101.85(5)
Co(2)–P(5)	2.2413(16)	N(3)–Co(2)–P(6)	130.76(13)
Co(2)–P(6)	2.2191(16)	N(3)–Co(2)–P(4)	109.05(12)
		P(6)–Co(2)–P(4)	104.75(6)
		N(3)–Co(2)–P(5)	103.55(12)
		P(6)–Co(2)–P(5)	102.51(7)
		P(4)–Co(2)–P(5)	102.95(7)

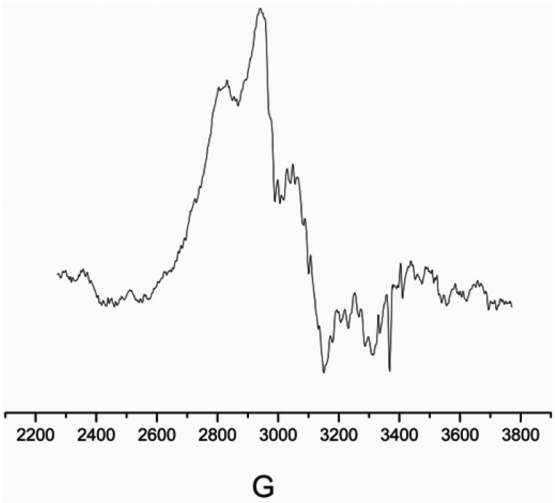

Fig. 2 EPR spectrum of **1** obtained in frozen toluene at 100 K.

117.68(19)°) that are greater than the P–Co–N angles (100.95(14)–103.85(14)°).

The Co–P bond lengths in the cation (2.1787(18)–2.2087(18) Å) are shorter than those found in the anion (2.3574(17) Å) reflecting the difference in charge between the anions.

The molar conductivity for **3** was found to be 129 S cm^2 M^{-1} (0.001 M, (CH_3CN, 25 °C). This is consistent with a 1 : 1 electrolyte.[18] The effective magnetic moment of **3** is 4.11μ_B (magnetic susceptibility balance at room temp.) in the solid state.

This is consistent with three unpaired electrons in a d^7 Co (II) anion with tetrahedral geometry. The most intense peak in ESI-MS positive mode corresponds to the $[CoH_2(PMe_3)_4]^+$ species, m/z = 365, and evidence for the $[Co(3,5\text{-}(CF_3)_2\text{-}Pz)_3(PMe_3)]^-$ species is found in the negative mode, m/z = 744. NMR spectroscopic data (C_6D_6) were consistent with the previous report of the diamagnetic cation, even in the presence of the paramagnetic anion. A broadened ^1H NMR spectrum was obtained only slightly shifted from the previously reported values for $[Co(PMe_3)_4H_2][BPh_4]$. The Co–H resonance is found as a broad singlet at −15.99 ppm, and two resonances are observed for the pairs of inequivalent PMe_3 groups at 0.22 and

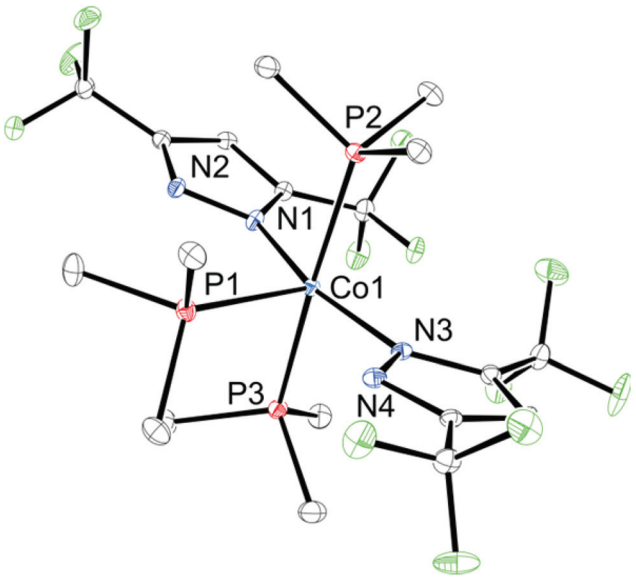

Fig. 3 Molecular structure and atom numbering scheme for $[Co(PMe_3)_3(3,5\text{-}(CF_3)_2\text{-}Pz)_2]$ (**2**). Thermal ellipsoids are scaled to the 30% probability level. Hydrogen atoms have been omitted for clarity.

Table 3 Selected bond lengths (Å) and angles (°) for **2**

Bond lengths		Bond angles	
Co(1)–N(3)	1.990(2)	N(3)–Co(1)–N(1)	164.60(9)
Co(1)–N(1)	1.991(2)	N(3)–Co(1)–P(3)	91.80(7)
Co(1)–P(3)	2.2548(8)	N(1)–Co(1)–P(3)	89.99(7)
Co(1)–P(2)	2.2703(8)	N(3)–Co(1)–P(2)	90.14(7)
Co(1)–P(1)	2.4772(8)	N(1)–Co(1)–P(2)	86.46(7)
		P(3)–Co(1)–P(2)	173.31(3)
		N(3)–Co(1)–P(1)	92.09(7)
		N(1)–Co(1)–P(1)	103.13(6)
		P(3)–Co(1)–P(1)	92.21(3)
		P(2)–Co(1)–P(1)	94.12(3)

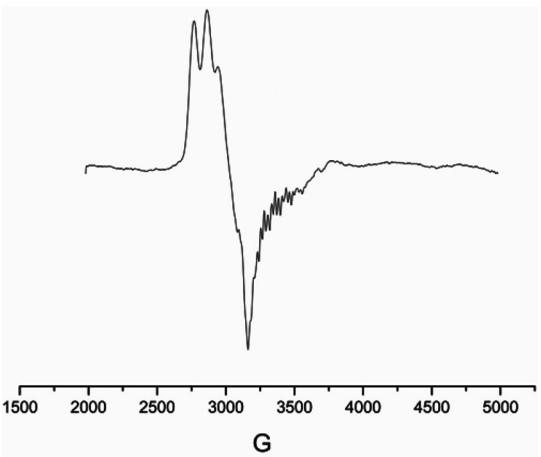

Fig. 4 EPR spectrum of **2** obtained in frozen toluene at 100 K.

0.46 ppm. The EPR spectrum of **3** is shown in Fig. 6. The spectrum is typical of rhombic symmetry with g = 2.07. The fine coupling to cobalt nuclei (I_{Co} = 7/2) is apparent, while

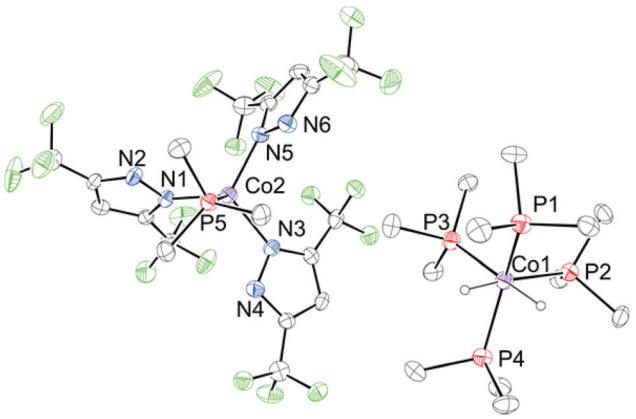

Fig. 5 ORTEP view of one of the two ion pairs of the asymmetric unit in [*cis*-Co$(PMe_3)_4H_2$][Co(PMe_3)(3,5-$(CF_3)_2$-Pz)$_3$] (**3**) showing the atom numbering scheme. Thermal ellipsoids are scaled to the 30% probability level. Metal hydrides shown for Co(1). All other hydrogen atoms have been omitted for clarity.

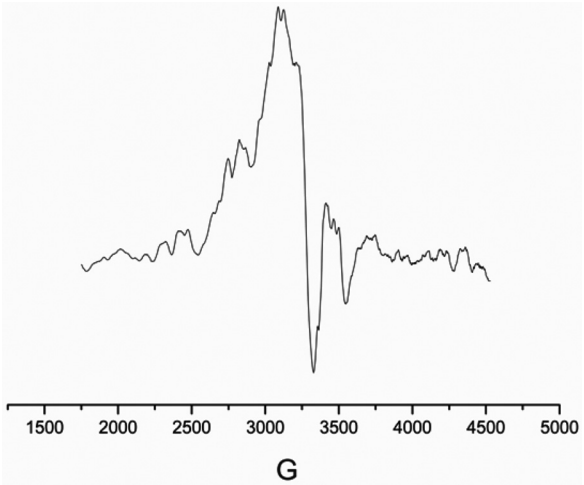

Fig. 6 EPR spectrum of **3** obtained in frozen toluene at 100 K.

Table 4 Selected bond lengths (Å) and angles (°) for **3**

Bond lengths		Bond angles	
Co(1)–P(1)	2.1787(18)	P(1)–Co(1)–H(2)	76.8(19)
Co(1)–P(4)	2.1810(18)	P(4)–Co(1)–H(2)	75.7(19)
Co(1)–P(3)	2.2063(17)	P(3)–Co(1)–H(2)	90.3(19)
Co(1)–P(2)	2.2087(18)	P(2)–Co(1)–H(2)	172.3(19)
Co(1)–H(1)	1.46(4)	H(1)–Co(1)–H(2)	88(2)
Co(1)–H(2)	1.43(5)	N(5)–Co(2)–N(3)	112.45(19)
Co(2)–N(5)	1.975(4)	N(5)–Co(2)–N(1)	116.09(18)
Co(2)–N(3)	1.996(4)	N(3)–Co(2)–N(1)	117.68(19)
Co(2)–N(1)	2.001(4)	N(5)–Co(2)–P(5)	103.85(14)
Co(2)–P(5)	2.3574(17)	N(3)–Co(2)–P(5)	102.94(14)
Co(3)–P(6)	2.1716(18)	N(1)–Co(2)–P(5)	100.95(14)
Co(3)–P(9)	2.176(2)	P(6)–Co(3)–P(9)	144.78(8)
Co(3)–P(7)	2.2007(18)	P(6)–Co(3)–P(7)	101.21(7)
Co(3)–P(8)	2.208(2)	P(9)–Co(3)–P(7)	102.84(7)
Co(3)–H(4)	1.55(5)	P(6)–Co(3)–P(8)	100.86(7)
Co(3)–H(3)	1.43(5)	P(9)–Co(3)–P(8)	100.37(8)
Co(4)–N(7)	1.985(4)	P(7)–Co(3)–P(8)	99.01(7)
Co(4)–N(9)	1.987(5)	P(6)–Co(3)–H(4)	77.9(18)
Co(4)–N(11)	1.997(5)	P(9)–Co(3)–H(4)	78.9(18)
Co(4)–P(10)	2.3585(18)	P(7)–Co(3)–H(4)	85.2(18)
		P(8)–Co(3)–H(4)	175.8(18)
P(1)–Co(1)–P(4)	143.59(7)	P(6)–Co(3)–H(3)	76.9(19)
P(1)–Co(1)–P(3)	102.66(7)	P(9)–Co(3)–H(3)	76.6(19)
P(4)–Co(1)–P(3)	100.92(7)	P(7)–Co(3)–H(3)	174.3(19)
P(1)–Co(1)–P(2)	101.83(7)	P(8)–Co(3)–H(3)	86.6(19)
P(4)–Co(1)–P(2)	102.22(7)	H(4)–Co(3)–H(3)	89(3)
P(3)–Co(1)–P(2)	97.33(7)	N(7)–Co(4)–N(9)	117.2(2)
P(1)–Co(1)–H(1)	73.8(16)	N(7)–Co(4)–N(11)	113.24(19)
P(4)–Co(1)–H(1)	81.6(16)	N(9)–Co(4)–N(11)	113.7(2)
P(3)–Co(1)–H(1)	176.3(16)	N(7)–Co(4)–P(10)	99.44(14)
P(2)–Co(1)–H(1)	84.8(16)	N(9)–Co(4)–P(10)	108.72(14)
		N(11)–Co(4)–P(10)	102.24(15)

hyperfine splitting from phosphorus (I_P = 1/2) and nitrogen nuclei (I_N = 1) is not well resolved.

The complex was tested for volatility in sealed tubes under vacuum (0.1 torr). Without melting, the complex slowly sublimed at 180 °C to afford blue prisms which were collected and subjected to X-ray diffraction analysis. This showed that **3** sublimes without decomposition as the ion pair. Decomposition was only observed at high temperature (>280 °C) under 1 atm of N_2 without melting.

[(3,5-$(CF_3)_2$-Pz)$_2$Co(μ-3,5-$(CF_3)_2$-Pz)(μ-$OPMe_3$)Li($OPMe_3$)$_2$] (4). The treatment of a diethyl ether suspension of two equivalents of 3,5-$(CF_3)_2$-PzLi with an *oxygenated* suspension of $CoCl_2$ and 3 equivalents of PMe_3 at −78 °C and a reaction time of 12 hours resulted in a suspension of NaCl and a blue solution. After filtration and removal of volatiles *in vacuo*, recrystallization from toluene–hexane (1 : 9) at −30 °C afforded blue prisms of **4** in 44% yield which were suitable for X-ray diffraction analysis. The initial experiments with this reaction system involved the presence of serendipitous oxygen. The isolation and characterization of **4** is reproducible provided that oxygen is present.

Complex **4** crystallizes in the monoclinic space group $P2_1/c$ with four independent molecules in the unit cell. The structure is shown in Fig. 7 with crystallographic details given in Table 1 and selected bond lengths and angles in Table 5. The two metal centers, Li and Co, are bridged by $OPMe_3$ and 3,5-$(CF_3)_2$-Pz with pseudo-tetrahedral geometry for both metals. A similar coordination scheme of heterobridged M–Li complexes with tetrahedral geometry is found in Ni(II) and Fe(II) complexes of the type [LM(μ-Pz)(μ-Cl)Li$(thf)_2$] (M = Fe, Ni, L = μ-diketiminate).[19] There is little distortion from ideal tetrahedral geometry for either metal center with N–Co–N and O–Li–O angles near ideal (113.94(11)–119.69(11)° and 109.7(3)–110.9(3)°, respectively). The Co–N bond length of the bridging 3,5-$(CF_3)_2$-Pz (2.006(3) Å) is longer than the non-bridging ligands (average 1.992(3) Å). A similar trend is found for the bridging Li–O bond length (2.034(6) Å) compared to the non-bridging $OPMe_3$ groups (1.886(6) Å). Complex **4** is formally a Co(II) species. The solid state effective magnetic moment (room temp.) is 4.211μ_B which is consistent with three unpaired electrons in a d^7 tetrahedral complex.

[(PMe_3)Co(μ-3,5-$(CF_3)_2$-Pz)$_2$(μ^3-OH)Li]$_2$ (5). In order to investigate the interactions of these Co pyrazolate complexes with other oxygen containing species we investigated the reaction of

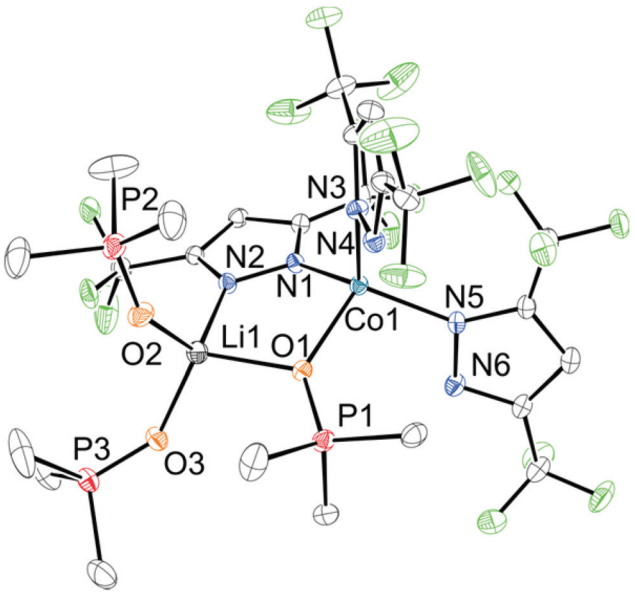

Fig. 7 Molecular structure and atom numbering scheme for $(3,5\text{-}(CF_3)_2\text{-}Pz)_2Co(\mu\text{-}3,5\text{-}(CF_3)_2\text{-}Pz)(\mu\text{-}OPMe_3)Li(OPMe_3)_2$ (**4**). Thermal ellipsoids are scaled to the 30% probability level. Hydrogen atoms have been omitted for clarity.

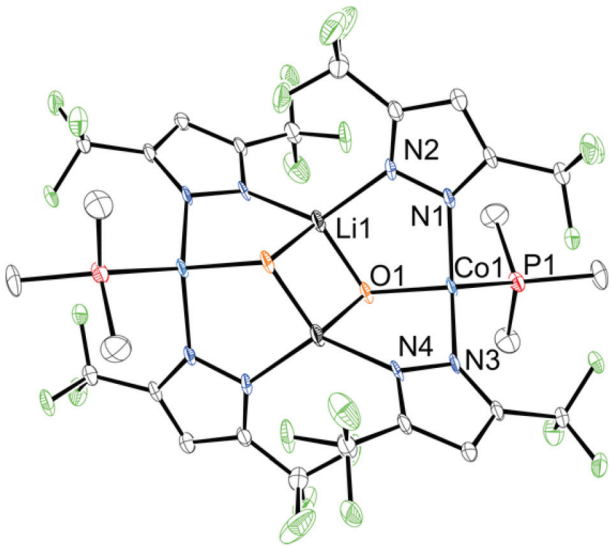

Fig. 8 Molecular structure and atom numbering scheme for $[(OPMe_3)Co(\mu\text{-}3,5\text{-}(CF_3)_2\text{-}Pz)_2(\mu^3\text{-}OH)Li]_2$ (**5**). Thermal ellipsoids are scaled to the 30% probability level. Hydrogen atoms have been omitted for clarity.

Table 5 Selected bond lengths (Å) and angles (°) for **4**

Bond lengths		Bond angles	
Co(1)–N(1)	2.006(3)	Co(1)–O(1)–Li(1)	107.16(19)
Co(1)–N(3)	1.993(3)	N(5)–Co(1)–N(3)	112.70(11)
Co(1)–N(5)	1.991(3)	N(5)–Co(1)–N(1)	119.69(11)
Co(1)–O(1)	1.994(2)	N(3)–Co(1)–N(1)	113.94(11)
Li(1)–O(2)	1.873(6)	N(5)–Co(1)–O(1)	105.17(10)
Li(1)–O(3)	1.899(6)	N(3)–Co(1)–O(1)	105.84(10)
Li(1)–O(1)	2.034(6)	O(1)–Co(1)–N(1)	96.65(10)
Li(1)–N(2)	2.082(6)	O(2)–Li(1)–O(3)	110.9(3)
P(1)–O(1)	1.524(2)	O(2)–Li(1)–O(1)	109.7(3)
P(2)–O(2)	1.486(3)	O(3)–Li(1)–O(1)	109.8(3)
P(3)–O(3)	1.494(2)	O(2)–Li(1)–N(2)	117.7(3)
		O(3)–Li(1)–N(2)	113.9(3)

Table 6 Selected bond lengths (Å) and angles (°) for **5**

Bond lengths		Bond angles	
Co(1)–O(1)	1.921(3)	O(1)–Co(1)–N(3)	99.53(16)
Co(1)–N(3)	2.018(4)	O(1)–Co(1)–N(1)	98.80(17)
Co(1)–N(1)	2.023(4)	N(3)–Co(1)–N(1)	117.23(18)
Co(1)–P(1)	2.3629(18)	O(1)–Co(1)–P(1)	109.95(12)
Co(1)–Li(1)#1	3.113(9)	N(3)–Co(1)–P(1)	120.99(13)
Co(1)–Li(1)	3.157(9)	N(1)–Co(1)–P(1)	107.42(13)
O(1)–Li(1)	1.904(10)	Li(1)–O(1)–Co(1)	111.3(3)
O(1)–Li(1)#1	2.007(10)	Li(1)–O(1)–Li(1)#1	83.0(4)
N(2)–Li(1)	2.047(10)	Co(1)–O(1)–Li(1)#1	104.8(3)
N(4)–Li(1)#1	2.067(10)	O(1)–Li(1)–O(1)#1	97.0(4)
		O(1)–Li(1)–N(2)	97.3(4)
		O(1)#1–Li(1)–N(2)	107.4(4)
		O(1)–Li(1)–N(4)#1	123.8(5)
		N(2)–Li(1)–N(4)#1	128.8(5)
		O(1)–Co(1)–N(1)	98.80(17)

the Co(II) bis-pyrazolate complex $Co(PMe_3)_3(3,5\text{-}(CF_3)_2\text{-}Pz)_2$ (**2**) with LiOH. The treatment of a suspension of LiOH in toluene with one equivalent of **2** and a reaction time of 12 hours resulted in a blue solution. Concentration and cooling of the solution to −30 °C afforded purple prisms of the hydroxide capped complex $[(PMe_3)Co(\mu\text{-}3,5\text{-}(CF_3)_2\text{-}Pz)_2(\mu^3\text{-}OH)Li]_2$ (**5**) in moderate yield (65%).

Complex **5** crystallizes in the triclinic space group $P\bar{1}$ with a crystallographic inversion center between the two Li centers resulting in one half of the molecule in the asymmetric unit and one independent molecule in the unit cell. The structure is shown in Fig. 8 with crystallographic details given in Table 1 and selected bond lengths and angles in Table 6. The complexation of LiOH results in the loss of two PMe_3 groups from each Co center. The crystallographically unique Co center adopts a distorted tetrahedral geometry which results in close interactions between CF_3 groups and the terminal PMe_3. The N–Li bond lengths in **5** average 2.057(10) Å and are similar to those in **4** (2.082(6) Å). There are many known examples of $Li_2(OH)_2$ ring systems and at least one in which the Li centers are also involved in bonding with bridging Pz groups. For example partial hydrolysis of the lithium salt of a $[t\text{BuB}(t\text{Bu-Pz})_3]^-$ affords a similar complex to **5**, $[(t\text{Bu})B(\mu\text{-}5\text{-}(t\text{Bu})\text{-}Pz)_2(\mu^3\text{-}OH)Li]_2$.[20] In this example the B-*t*Bu center, instead of the Co-PMe_3 moiety in **5**, does not appreciably alter the tetrahedral geometry found for the Li and O centers. The pyrazolate N–Li distances are consistent with those found in **4** and **5**.

Complexation of LiOH by **2** does not alter the oxidation state of the Co(II) center in **5**. However the geometry changes from square pyramidal to tetrahedral. The effective magnetic moment ($6.63\mu_B$) measured in the solid state (room temp.) is consistent with six unpaired electrons expected for two d^7

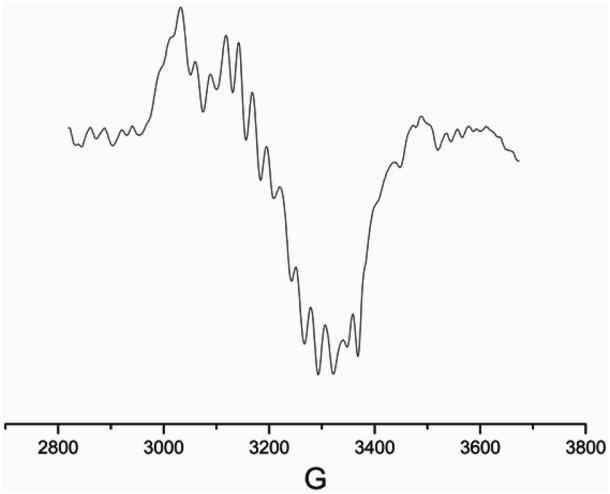

Fig. 9 EPR spectrum of **5** obtained in frozen toluene at 100 K.

tetrahedral centers (3 unpaired electrons per Co). The EPR spectrum of **5** obtained in frozen toluene at 100 K is shown in Fig. 9 (g = 2.09). The fine coupling to the Co nuclei (I_{Co} = 7/2) is well resolved along with some hyperfine spin–orbit coupling, likely due to interactions with the P nuclei (I_P = 1/2), as coupling of the two equivalent N nuclei (I_N = 1) would result in a more complicated spectrum. **5** was a high melting solid and showed no signs of volatility.

$[Co(OPMe_3)_2(3,5\text{-}(CF_3)_2\text{-}Pz)_2]$ (6). In contrast to the reaction of **2** with LiOH, the treatment of a toluene solution of **2** with O_2 for 5 minutes resulted in a color change of the solution from blue to purple. Concentration of this solution and cooling to −30 °C afforded large blue prisms of the mononuclear phosphine oxide complex, $Co(OPMe_3)_2(3,5\text{-}(CF_3)_2\text{-}Pz)_2$ (**6**), in 74% yield. This complex is also formed by treatment of a toluene solution of $[Co(PMe_3)_4H_2][Co(PMe_3)(3,5\text{-}(CF_3)_2\text{-}Pz)_3]$ (**3**) with O_2 in 38% yield.

Complex **6** crystallizes in the triclinic space group $P\bar{1}$ with two independent molecules in the unit cell. The structure is shown in Fig. 10 with crystallographic details given in Table 1 and selected bond lengths and angles in Table 7. The structure features a tetrahedral Co center with distortion of the N(1)–Co(1)–N(3) bond angle (117.1(3)°) resulting in a slight distortion of the other bond angles (107.0(3)°–108.9(2)°).

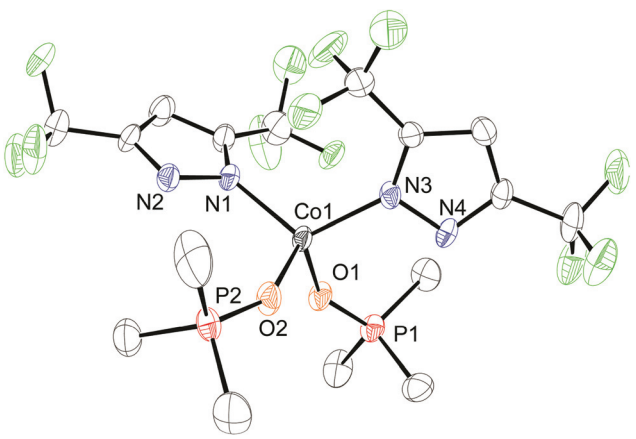

Fig. 10 Molecular structure and atom numbering scheme for $[Co(OPMe_3)_2(3,5\text{-}(CF_3)_2\text{-}Pz)_2]$ (**6**). Thermal ellipsoids are scaled to the 30% probability level. Hydrogen atoms have been omitted for clarity.

Table 7 Selected bond lengths (Å) and angles (°) for **6**

Bond lengths		Bond angles	
Co(1)–O(1)	1.949(5)	O(2)–Co(1)–O(1)	107.0(3)
Co(1)–O(2)	1.944(5)	O(2)–Co(1)–N(3)	107.7(3)
Co(1)–N(1)	1.984(6)	O(1)–Co(1)–N(3)	108.3(2)
Co(1)–N(3)	1.983(6)	O(2)–Co(1)–N(1)	108.9(2)
P(1)–O(1)	1.502(5)	O(1)–Co(1)–N(1)	107.3(3)
P(2)–O(2)	1.490(6)	N(3)–Co(1)–N(1)	117.1(3)

Catalysis of the oxidation of phosphines to phosphine oxides with Co complexes with high turnover numbers is well known.[21,22] Thus the conversion of **2** to **6** is not surprising. The chloride analogue of **6**, $Co(OPMe_3)_2Cl_2$ is known and has been the subject of more than one crystallographic study[23,24] and the Co–O distances and angles similar to those found in **6**. The effective magnetic moment of **6** is 4.43μ_B, in the solid state at room temperature and is consistent with three unpaired electrons in a d^7 tetrahedral complex. The EPR spectrum in frozen toluene at 100 K showed a broad signal at g = 2.23 (ESI†). Complex **6** was tested for volatility in a sealed tube under vacuum (0.1 torr). Heating to 140 °C resulted in sublimation to afford crystals suitable for X-ray diffraction analysis which revealed that the complex was unchanged after sublimation.

Conclusions

The synthesis and characterization of a series of cobalt complexes containing the bis-trifluoromethyl-pyrazolate ligand is reported. Although several complexes were found to have volatilities and thermal stabilities that made them suitable as potential CVD precursors our preliminary studies have been hampered by the extreme air sensitivity of these compounds. Preliminary film growth studies will be reported separately.

Experimental

General procedures

All reactions were performed under a dry, oxygen-free nitrogen atmosphere or under vacuum using standard Schlenk line and dry box techniques. Solvents were dried prior to use by distillation from sodium benzophenone ketyl anion under nitrogen. The compounds 3,5-bis(trifluoromethyl)pyrazole 3,5-$(CF_3)_2$-PzH,[25] $[Co(PMe_3)_4]$,[26] and $[Co(PMe_3)_3Cl]$[25] were prepared as previously described. Trimethylphosphine (97%), sodium hydride, and n-butyl lithium (1.6 M in hexane) were purchased from Aldrich and used without further purification. EPR data were collected on a Bruker EMX Plus X-band spectrometer with 4 mW microwave power and 0.1 G modulation amplitude

with a liquid nitrogen cooled cryostat. NMR spectra were recorded on a Varian 300 Unity spectrometer (^{1}H, 300 MHz; ^{19}F, 282 MHz; ^{31}P, 121 MHz) at 25 °C. ^{1}H NMR signals are reported relative to residual proton resonances in deuterated solvents. Electrospray Ionization (ESI) mass spectra were recorded on a Thermo-Fisher LTQ. Infrared spectra were recorded using a Nicolet IR 200 FTIR spectrometer using attenuated total reflectance (ATR). Microanalysis (C, H, N) were performed by Galbraith Laboratories of Knoxville, TN or QTI Labs of Whitehouse, NJ. Melting points were obtained using an Electrothermal resistively heated melting point apparatus in sealed glass capillaries under a dinitrogen atmosphere or 0.1 torr vacuum.

Single crystal X-ray crystallography

All crystals were mounted on a glass fiber. The data was collected on either a Nonius Kappa CCD diffractometer using a graphite monochromator with MoKα radiation (λ = 0.71073 Å) at reduced temperature using an Oxford Cryostream low temperature device or a Rigaku AFC12 diffractometer with a Saturn 724+ CCD using a graphite monochromator with MoKα radiation at reduced temperature using a Rigaku XStream low temperature device. Data reduction was performed with either DENZO-SMN or Rigaku Americas Corporation's Crystal Clear version 1.40. The structures were solved by direct methods using SIR97 and refined by full-matrix least-squares on F^2 with anisotropic displacement parameters for the non-H atoms using SHELXL-97. The absolute configuration was assigned by internal comparison to the known absolute configuration of selected portions of the molecule. The hydrogen atoms on carbon were calculated in idealized positions with isotropic displacement parameters set to 1.2 × U_{eq} of the attached atom (1.5 × U_{eq} for methyl hydrogen atoms). The function, $\Sigma w(|F_o|^2 - |F_c|^2)^2$, was minimized, where $w = 1/[(\sigma(F_o))^2 + (0.0528 \times P)^2 + (0.685 \times P)]$ and $P = (|F_o|^2 + 2|F_c|^2)/3$. Neutral atom scattering factors and values used to calculate the linear absorption coefficient are from the International Tables for X-ray Crystallography (1992).[27] All figures were generated using SHELXTL/PC.

Synthesis of complexes

[Co(PMe$_3$)$_3$(3,5-(CF$_3$)$_2$-Pz)] (1). A solution of 3,5-(CF$_3$)$_2$-PzH (0.091 g 0.446 mmol) in hexane (50 ml) was added to a suspension of NaH (0.126 g, 0.525 mmol) in hexane (50 ml) at 25 °C and stirred for 8 hours. A suspension of [Co(PMe$_3$)Cl] (0.141 g, 0.437 mmol) in hexane (100 ml) was then added to the suspension and stirred 12 hours during which time it changed in color from dark to bright blue and a cloudy white precipitate was formed. The solution was filtered and the filtrate was evaporated to dryness. The residue was sublimed onto a cold finger cooled with dry ice/acetone under static vacuum (0.1 torr) at 110 °C to afford **1** as the sublimate. The sublimate was recovered in the glove box under N_2. Crystals suitable for X-ray analysis were grown in a zone sublimator under vacuum (0.1 torr) at 120 °C over 36 hours. Isolated yield: 0.145 g, 68%. M.p. 80–82 °C (1 atm N_2), 108–110 °C sublime (0.1 torr). μ_{eff} = 3.055μ_B. FTIR (ATR, cm^{-1}): 2970 vw, 2905 vw, 1535 vw, 1498 w, 1425 w, 1298 vw, 1298 w, 1284 w, 1252 s, 1203 w, 1146 m, 1109 vs, 1065 w, 1010 w, 998 m, 974 m, 937 vs, 862 w, 798 m, 716 m. EI/MS *m*/*z*: 287 [M$^+$, -Pz], 211 [M$^+$, -PMe$_3$, -Pz]. Anal. Found: C, 32.0; H, 5.6; N, 5.2. Calc: C, 34.3; H, 5.8; N, 5.7.

[*cis*-Co(PMe$_3$)$_3$(3,5-(CF$_3$)$_2$-Pz)$_2$] (2). A solution of 3,5-(CF$_3$)$_2$-PzH (0.80 g 3.92 mmol) in hexane (100 ml) was added to a suspension of NaH (0.094 g, 3.92 mmol) in hexane (50 ml) at 25 °C and stirred for 8 hours. In a separate flask, PMe$_3$ (0.447 g, 5.88 mmol) was added dropwise to a suspension of $CoCl_2$ (0.25 g, 1.96 mmol) in hexane (100 ml). This suspension was then added to the suspension of 3,5-(CF$_3$)$_2$-PzNa at 25 °C and stirred for 12 hours. The solution was filtered and the filtrate evaporated to dryness. The residue was extracted with hexane (250 ml) and filtered. The volume of the filtrate was reduced *in vacuo* (175 ml), and cooling (−30 °C) gave large brown prisms of **2** suitable for X-ray analysis. Isolated yield: 0.78 g, 58%. M.p. 69–72 °C (1 atm N_2). μ_{eff} = 1.99μ_B. FTIR (ATR, cm^{-1}): 2910 vw, 1521 w, 1502 w, 1418 w, 1344 w, 1256 s, 1206 m, 1148 m, 1113 vs, 1076 m, 1003 s, 977 m, 946 s, 853 w, 803 w, 755 w, 732 w, 710 w. EI/MS *m*/*z*: 490 [M$^+$, -Pz], 414 [M$^+$, -PMe^3, -Pz]. Anal. Found: C, 32.2; H, 3.9; N, 8.3. Calc: C, 32.9; H, 4.2; N, 8.1.

[Co(PMe$_3$)$_4$H$_2$][Co(PMe$_3$)(3,5-(CF$_3$)$_2$-Pz)$_3$] (3). A solution of 3,5-(CF$_3$)$_2$-PzH (0.317 g, 1.553 mmol) in diethyl ether (60 ml) was added to a stirred solution of [Co(PMe$_3$)$_4$] (0.217 g, 0.598 mmol) in diethyl ether (50 ml) at 25 °C and stirred for 8 hours. The color of the solution quickly changed from black to green and then blue. Volatile materials were removed *in vacuo* and the residue was extracted into a toluene–diethyl ether mixture (9 : 1, 40 ml) and filtered. Cooling to −30 °C gave large purple prisms of **3** suitable for X-ray analysis. Isolated yield: 0.492 g, 74%. M.p. >280 °C (dec.) (1 atm N_2), 180–185 °C sublime (0.1 torr); μ_{eff} = 4.12μ_B. Λ_M (0.001 M, CH_3CN): 129 S cm^2 M^{-1}. ^{1}H NMR (300 MHz, C_6D_6) δ −15.99 (br s, 2 H, Co-*H*), 0.22 (s, 9 H, P-C*H*$_3$), 0.46 (s, 9 H, P-C*H*$_3$). FTIR (ATR, cm^{-1}): 2978 vw, 1945 vw, 1540 vw, 1498 w, 1423 w, 1346 w, 1308 w, 1292 w, 1256 s, 1212 m, 1112 vs, 1069 m, 1009 s, 975 m, 941 m, 861 w, 802 m, 754 w, 727 w. EI/MS *m*/*z*: 365 [Co(PMe$_3$)$_4$H$_2^+$], 337 [Co(PMe$_3$)Pz$^+$]. Anal. Found: C, 31.3; H, 4.3; N, 6.8. Calc: C, 32.4; H, 4.5; N, 7.5.

(3,5-(CF$_3$)$_2$-Pz)$_2$Co(μ-3,5-(CF$_3$)$_2$-Pz)(μ-OPMe$_3$)Li(OPMe$_3$)$_2$ (4). A solution of *n*-BuLi (1.20 ml, 1.6 M in hexane) was added dropwise to a solution of 3,5-(CF$_3$)$_2$-PzH (0.39 g 1.911 mmol) in diethyl ether (30 ml) at −78 °C. The mixture was stirred and allowed to warm slowly to room temp. (1 h). In a separate flask, PMe$_3$ (0.28 ml, 2.867 mmol) was added dropwise to a suspension of $CoCl_2$ (0.123 g, 0.956 mmol) in diethyl ether (100 ml) followed by bubbling O_2 through the solution for 30 seconds. The flask was cooled to −78 °C and 3,5-(CF$_3$)$_2$-PzLi was added. The suspension was allowed to warm slowly to room temperature and stirred for 12 h. during which time it changed in color from purple to blue and a cloudy white precipitate formed. The solution was filtered and the filtrate evaporated to dryness. The residue was extracted into a hexane–toluene mixture (9 : 1, 60 ml) and cooled (−30 °C) to give blue

prisms of **4** suitable for X-ray analysis. Isolated yield: 0.410 g, 44%. M.p. 122–125 °C (1 atm N_2). μ_{eff} = 4.211μ_B. FTIR (ATR, cm^{-1}): 1531 w, 1500 w, 1422 vw, 1346 w, 1313 w, 1298 w, 1257 m, 1214 w, 1193 m, 1159 m, 1113 vs, 1089 m, 1074 w, 1011 m, 976 w, 941 m, 857 w, 806 m, 755 w. EI/MS *m*/*z*: 656 [$CoPz_2(OPMe_3)_2Li^+$], 486 [$LiPz(OPMe_3)_3^+$] 262 [$CoPz^+$]. Anal. Found: C, 30.4; H, 3.7; N, 7.9. Calc: C, 30.3; H, 3.2; N, 8.8.

[(PMe$_3$)Co(μ-3,5-(CF$_3$)$_2$-Pz)$_2$(μ^3-OH)Li]$_2$ (5). A solution of **2** (0.41 g, 0.591 mmol) in toluene (50 ml) was added to a suspension of LiOH (0.014 g, 0.591 mmol) in toluene (50 ml) at room temperature and the mixture stirred for 12 hours. The volume was reduced under vacuum (60 ml) and cooled (−30 °C) to yield small purple prisms of **5** suitable for X-ray analysis. Isolated yield: 0.218 g, 65%. M.p. 197–200 °C (1 atm N_2). μ_{eff} = 6.63μ_B. FTIR (ATR, cm^{-1}): 3586 w, 1532 w, 1504 w, 1426 vw, 1352 w, 1291 w, 1258 s, 1217 m, 1148 m, 1112 vs, 1090 m, 1012 s, 985 w, 976 w, 942 m, 858 w, 810 w, 748 w. EI/MS *m*/*z*: 850 [$Co_2Pz_3(LiOH)_2PMe_3^+$], 986 [$Co_2Pz_4(LiOH)_2PMe_3^+$, -CF_3]. Anal. Found: C, 26.7; H, 2.2; N, 9.1. Calc: C, 27.6; H, 2.1; N, 9.9.

[Co(OPMe$_3$)$_2$(3,5-(CF$_3$)$_2$-Pz)$_2$] (6). Method A: oxygen gas (1 atm) was bubbled through a solution of **2** (0.25 g, 0.361 mmol) in toluene (50 ml) for 5 minutes. The volume of the solution was reduced *in vacuo* and the flask cooled (−30 °C) to give large blue prisms of **6** suitable for X-ray analysis. Isolated yield: 0.173 g, 74%.

Method B: oxygen gas (1 atm) was bubbled through a solution of **3** (0.20 g, 0.180 mmol) in toluene (50 ml) for 10 minutes. The solution was stirred for 8 hours at room temperature and cooled (−30 °C) to give large blue prisms of **6** suitable for X-ray analysis. Isolated yield: 0.089 g, 38%. M. p. 93–96 °C (1 atm N_2); 140–145 °C sublime (0.1 torr). μ_{eff} = 4.43μ_B. FTIR (ATR, cm^{-1}): 2963 vw, 1526 vw, 1499 vw, 1422 vw, 1312 w, 1298 w, 1258 s, 1216 w, 1067 vs, 1074 m, 1011 vs, 976 m, 950 m, 860 m, 798 s, 753 m. EI/MS *m*/*z*: 446 [$CoPz(OPMe_3)_2^+$], 262 [$CoPz^+$]. Anal. Found: C, 28.6; H, 2.8; N, 8.2. Calc: C, 29.6; H, 3.1; N, 8.6.

Acknowledgements

The authors would like to thank the Welch Foundation (Grant F-816) and the Petroleum Research Fund, administered by the American Chemical Society (47014-ACS) for financial support. X-ray data was collected on instrumentation purchased with funds from NSF grant #0741973.

Notes and references

1 M. Paunovic, P. J. Bailey, R. G. Schad and D. A. Smith, *J. Electrochem. Soc.*, 1994, **141**, 1843.
2 L. B. Henderson and J. G. Ekerdt, *Microelectron. Eng.*, 2010, **87**, 588.
3 L. B. Henderson and J. G. Ekerdt, *J. Electrochem. Soc.*, 2010, **157**, D29.
4 L. B. Henderson, J. H. Rivers, D. E. Bost, R. A. Jones and J. G. Ekerdt, *J. Vac. Sci. Technol.*, 2010, **28**(1), 54–60.
5 G. A. West and K. W. Beeson, *Appl. Phys. Lett.*, 1988, **53**, 740.
6 G. J. M. Dormans, G. J. B. M. Meekes and E. G. J. Staring, *J. Cryst. Growth*, 1991, **114**, 364.
7 R. G. Charles and P. G. Haverlack, *J. Inorg. Nucl. Chem.*, 1969, **31**, 995.
8 A. Gulino, G. Fiorito and I. Fragala, *J. Materi. Chem.*, 2003, **13**, 861.
9 H. Choi and S. Park, *Chem. Mater.*, 2003, **15**, 3121.
10 S. Mather, C. Cavelius and H. Shen, *Z. Anorg. Allg. Chem.*, 2009, **635**, 2106.
11 A. A. Tahir, K. C. Molloy, M. Mazhar, G. Kociok-Köhn, M. Hamid and S. Dastgir, *Inorg. Chem.*, 2005, **44**, 9207.
12 J. Shin, A. Waheed, K. Agapiou, W. A. Winkenwerder, H.-W. Kim, R. A. Jones, G. S. Hwang and J. G. Ekerdt, *J. Am. Chem. Soc.*, 2006, **128**, 16510–16511.
13 J. Shin, A. Waheed, W. A. Winkenwerder, H.-W. Kim, K. Agapiou, R. A. Jones, G. S. Hwang and J. G. Ekerdt, *Thin Solid Films*, 2007, **515**, 5298–5307.
14 W. Jeffrey McCarty, X. Yang, L. J. DePue Anderson and R. A. Jones, *Dalton Trans.*, 2012, **41**(1), 173–179.
15 J. H. Rivers, L. J. DePue Anderson, C. M. N. Starr and R. A. Jones, *Dalton Trans.*, 2012, **41**, 5401–5408.
16 Y. Peres, M. Dartiguenave, Y. Dartiguenave, J. F. Britten and A. L. Beauchamp, *Organometallics*, 1990, **9**, 1041.
17 M. Paneque, S. Sirol, M. Trujillo, E. Carmona, E. Gutiérrez-Puebla, M. A. Monge, C. Ruiz, F. Malbosc, C. S.-L. Berre, P. Kalck, M. Etienne and J. C. Daran, *Chem.–Eur. J.*, 2001, **7**, 3868.
18 W. J. Geary, *Coord. Chem. Rev.*, 1971, **7**, 81.
19 J. Vela, S. Vaddadi, S. Kingsley, C. J. Flaschenriem, R. J. Lachicotte, T. R. Cundari and P. L. Holland, *Angew. Chem., Int. Ed.*, 2006, **45**, 1607.
20 O. Graziani, P. Hamon, J.-Y. Thépot, L. Toupet, P. Á. Szilágyi, G. Molnár, A. Bousseksou, M. Tilset and J.-R. Hamon, *Inorg. Chem.*, 2006, **45**, 5661.
21 K. Yamamoto, *Polyhedron*, 1986, **5**, 913.
22 Y. H. Hwang and C. P. Cheng, *J. Chem. Soc., Chem. Commun.*, 1992, 317.
23 F. Edelmann and U. Behrens, *Acta Crystallogr., Sect. C: Cryst. Struct.Commun.*, 1986, **42**, 1715.
24 M.-J. Menu, M. Simard, A. L. Beauchamp, H. Konig, M. Dartiguenave, Y. Dartiguenave and H.-F. Klein, *Acta Crystallogr., Sect. C: Cryst. Struct. Commun.*, 1989, **45**, 1697.
25 O. Renn, L. M. Venanzi, A. Marteletti and V. Gramlich, *Helv. Chim. Acta*, 1995, **78**, 993.
26 H. F. Klein and H. H. Karsch, *Chem. Ber.*, 1975, **108**, 944.
27 *International Tables for X-ray Crystallography*, ed. A. J. C. Wilson, vol. C, 1992.